Parametric Study of Cohesive ITZ in Meso-scale Concrete Model

DOI:
10.1016/j.prostr.2020.01.081

Document Version
Final published version

Available online at www.sciencedirect.com

ScienceDirect

Procedia Structural Integrity 23 (2019) 167–172

Structural Integrity Procedia

www.elsevier.com/locate/procedia

9th International Conference on Materials Structure and Micromechanics of Fracture

Parametric Study of Cohesive ITZ in Meso-scale Concrete Model

Jiaming Wang[a,*], Andrey P Jivkov[a], Dirk L Engelberg[b], Q.M. Li[a]

[a]*School of Mechanical, Aerospace and Civil Engineering, University of Manchester, Manchester, UK*
[b]*Materials Performance Centre, School of Materials, University of Manchester, Manchester, UK*

Abstract

Modelling of concrete at the meso-scale provides an effective way to analyse the effects of its constituents on damage initiation and evolution, leading to better understanding and predicting structural integrity. Majority of works to date focus on models calibration and validation with experiments in either tension or compression, leaving open the question of how such models perform under complex stress states. This work presents a modelling approach that includes all key constituents of the concrete meso-structure: coarse aggregates, represented by inclusions with elastic-brittle behaviour, mortar (including cement, sand and fine aggregates), represented with plastic-damage behaviour, interfacial transition zones (ITZ) between aggregates and mortar, represented by zero-thickness cohesive interfaces, and air voids or pores. Tension and compression experiments with mortar specimens are conducted to obtain its plastic-damage constitutive law. Similar experiments with concrete with several aggregate volume fractions are conducted to obtain stress-strain behaviours for further calibration of cohesive laws and model validation. Numerical simulations show that the proposed approach with pre-calibration of mortar behaviour leads to very good agreements between the predictions of the concrete meso-structural models and the experimental results under both tension and compression. The calibration of ITZ cohesive laws is performed by a parametric study of the effects of critical stress and fracture energy on the predicted stress-strain curves and fracture patterns. The results are used to propose a practical set of ITZ cohesive parameters.

Keywords: Concrete meso-structure; Cohesive interfaces; Critical stress; Fracture energy; Failure patterns

1. Introduction

Concrete is a composite material, which demands some explicit representation of its heterogeneous composition for understanding the initiation and evolution of localised phenomena, such as damage and fracture. At the largest length scale with observable heterogeneities, called the meso-scale, the concrete constituents are: coarse aggregates, mortar (cement with sand and fine aggregates embedded) and air voids entrapped in the mortar. Aggregates are elastic-brittle stones, gravel or crashed, but their strength is higher than the stresses reached at concrete failure. As they remain in elastic regime, aggregates are represented as elastic inclusions with their specific stiffness. Mortar is modelled as a homogeneous continuum with elastic-plastic or elastic-plastic-damage behaviour to represent the processes of slip

* Corresponding author.
E-mail address: jiaming.wang@manchester.ac.uk

2452-3216
10.1016/j.prostr.2020.01.081

and re-arragement of its constituents. The latter representation is used here. In addition to these meso-constituents, it is known that aggregates are coated with higher-porosity mortar with distinct properties, which is referred to as interfacial transition zones (ITZ) with typical thickness between 10 and 100 μm [1, 2]. Having lower stiffness and strength than mortar, ITZ provide both preferable locations for damage initiation and easier pathways for crack development.

The physical ITZ thickness is negligible in comparison with coarse aggregates, which makes ITZ models with physical thickness computationally demanding, sometimes prohibitively. This is presently tackled by representing ITZ as zero-thickness interfaces between aggregates and mortar, modelled computationally by cohesive elements [3–7]. Key parameters of ITZ cohesive laws, such as stiffness, critical strength and fracture energy, in both normal and shear directions, cannot be determined readily with existing experimental techniques. Therefore a combination of judgment as to how these differ from the mortar and parametric studies is used for their calibration. Selection of appropriate parameters is made by comparisons with experimentally observed macroscopic behaviour, including stress-strain curves and crack patterns. Previous works have demonstrated calibration of cohesive laws with experiments in either tension [3–6] or compression [7]. However, there is no work demonstrating the performance of calibrated cohesive laws under both tension and compression, which is an essential condition for using this type of meso-structure models under complex stress states existing in real engineering structures. One critical element of the meso-structure - elastic aggregates, plastic-damage mortar, cohesive ITZ - is the very distinct behaviour of mortar under tension and compression. Its proper determination appears to be key to the successful modelling of concrete under complex stresses.

The aim of this paper is to clarify the effect of ITZ cohesive parameters on predicted concrete behaviour, when the properties of the other constituents are determined by experiments. It is shown that the mortar plastic-damage behaviour has the strongest influence on the energy dissipation and overall stress-strain behaviour under both tension and compression. The effect of ITZ parameters is limited to the post-peak softening branch and the crack patterns.

2. Experimental and modelling background

Quasi-static experiments were carried out on mortar and concrete specimens: cylindrical specimens with diameter 100 mm and height 200 mm were tested in compression, dogbone specimens were tested in tension. Limestone aggregates with sieve size distribution between 6.3 and 10 mm were used for concrete samples. These were prepared with 40% aggregate volume fractions. Mortar specimens had the same water-cement-sand mixes as the ones used for concrete samples. Detailed experiment design will be presented elsewhere. 3D meso-structures were generated within prescribed volumes by random distribution of spherical aggregates with sizes selected from the sieve distribution and voids with 1% volume fraction. The generation used the 'take-and-place' procedure described in detail in [8]. For this work, the meso-structures covered cylindrical volumes with diameter of 50 mm and height of 100 mm due to the computational cost if modelling the original cylinder. The same cylinders were adopted under tension, because direct tension test with cylinder was experimentally challenging and dogbone samples were applied for standard tension experiments. The volumes were tessellated into voxels in preparation for meshing used in image-based modelling. Voxel size of 0.25 mm was adopted after mesh sensitivity test. Tetrahedral meshes, covering aggregates and mortar phases were derived and an in-house procedure was used to insert zero-thickness cohesive elements (CE) at the aggregate-mortar interfaces to represent ITZ.

The concrete-damage-plasticity (CDP) model is adopted for the constitutive law of mortar, because mortar can be considered as a lower-scale concrete. Under compression, the stress-strain response can be classified into four stages: linear elasticity, plasticity, strain hardening up to onset of damage and strain softening. The full expression is described by Equation (1) [9], where σ_c and ε_c are the current compressive stress and strain, respectively, σ_{c0} and ε_{c0} are the peak stress and corresponding strain, respectively, and ε_{cu} is the strain at damage initiation, α_a and α_d are coefficients related with σ_{cu}. Under tension, the stress-strain relation is linear up to the peak stress, while the post peak behaviour can be expressed by Equation (2) [9], where α_t is a coefficient related with σ_{t0}.

$$\frac{\sigma_c}{\sigma_{cu}} = \begin{cases} \frac{E_0\varepsilon_c}{\sigma_{cu}}, & \frac{\sigma_c}{\sigma_{c0}} \le 0.4 \\ \alpha_a \frac{\varepsilon_c}{\varepsilon_{cu}} + (3-2\alpha_a)\left(\frac{\varepsilon_c}{\varepsilon_{cu}}\right)^2 + (\alpha_a - 2)\left(\frac{\varepsilon_c}{\varepsilon_{cu}}\right)^3, & \frac{\sigma_c}{\sigma_{c0}} \ge 0.4 \;\&\; \frac{\varepsilon_c}{\varepsilon_{cu}} \le 1 \\ \frac{\frac{\varepsilon_c}{\varepsilon_{cu}}}{\alpha_d\left(\frac{\varepsilon_c}{\varepsilon_{cu}} - 1\right)^2 + \frac{\varepsilon_c}{\varepsilon_{cu}}}, & \frac{\varepsilon_c}{\varepsilon_{cu}} \ge 1 \end{cases} \tag{1}$$

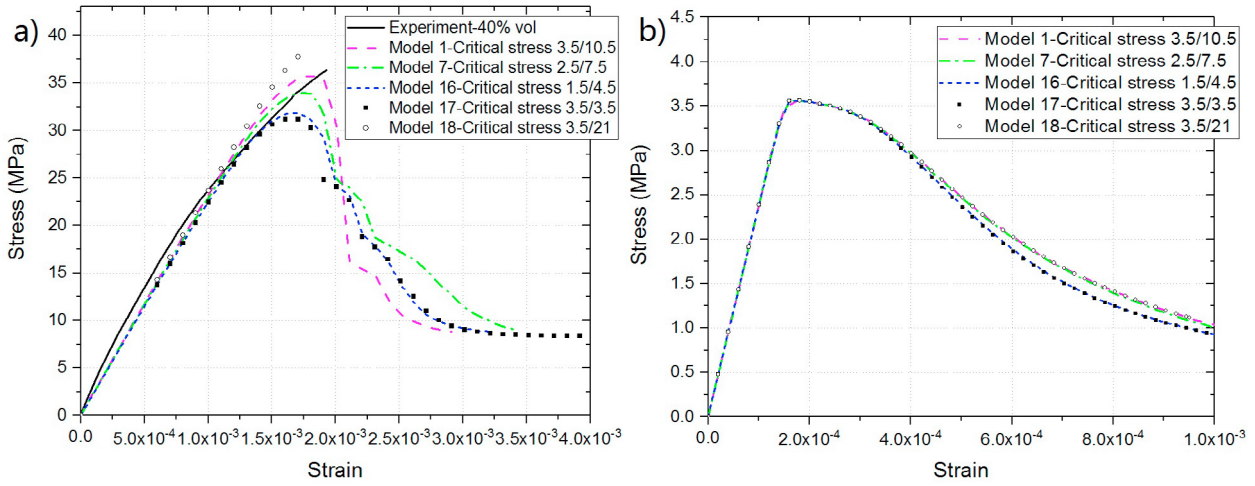

Fig. 1. Stress-strain curves obtained with variable ITZ cohesive strength under compression (a) and tension (b)

Table 1. Parameters of cohesive zone model for ITZ

Model Number	1	7	16	17	18	9	10	19	20
Cohesive strength MPa	3.5/10.5	2.5/7.5	1.5/4.5	3.5/3.5	3.5/21	3.5/10.5	3.5/10.5	3.5/10.5	3.5/10.5
Fracture energy N/mm	0.03/0.09	0.03/0.09	0.03/0.09	0.03/0.09	0.03/0.09	0.01/0.03	0.05/0.15	0.03/0.18	0.03/0.3

Young's modulus and Poisson's ratio of limestone aggregates were taken from [10] - 45 GPa and 0.2, respectively. Compression and tension experiment results for mortar provided Young's modulus of 20 GPa, compressive strength of 56 MPa and and tensile strength of 3.7 MPa. These were used to calibrate the CDP model.

$$\frac{\sigma_t}{\sigma_{t0}} = \frac{\frac{\varepsilon_t}{\varepsilon_{t0}}}{\alpha_t\left(\frac{\varepsilon_t}{\varepsilon_{t0}} - 1\right)^{1.7} + \frac{\varepsilon_t}{\varepsilon_{t0}}} \tag{2}$$

CE representing ITZ used a traction-separation law described in [5]. The CE stiffness is set to be 10^5 MPa/mm [8]. The critical traction in normal mode (normal strength) cannot exceed the tensile strength of mortar, so a set of critical tractions between 1.5 and 3.5 MPa were tested. The ITZ fracture energy in normal mode is lower than the mortar due to higher porosity of ITZ. A set of fracture energies between 0.01 and 0.05 N/mm were tested. In a number of previous works, the normal and shear modes strength and fracture energy were assumed to be the same [4–6]. However, based on experimental evidence, [7] adopted significantly larger shear strength and fracture energy, specifically between three and ten times larger. Three times larger shear strength and energy are adopted in this work. The combinations used in simulations presented in the next section are shown in Table 1, where the first and second numbers denote the normal and shear values, respectively. Specimens were loaded via displacements parallel to the cylinder axis prescribed at the two circular surfaces. Displacements at one of the surfaces were zero. At the other surface displacements were given at surface nodes in tension, and via a rigid plate in compression. After testing different model realisations, i.e. different spatial distributions of aggregates, and knowing that the stress-strain curves were the same, one representative realisation was selected to carry out all simulations in both tension and compression.

3. Results and discussion

Results obtained with variable normal cohesive strength under compression and tension are presented as follows. Fig. 1 shows the stress-strain curves together with the experimental results. Fig. 2 shows energy dissipations in mortar and ITZ, where DMD and PD corresponds to damage and plastic dissipation energy. Fig. 3 shows the crack patterns assuming a damage factor SDEG > 0.9 under compression and SDEG > 0.5 under tension, where SDEG=1 means

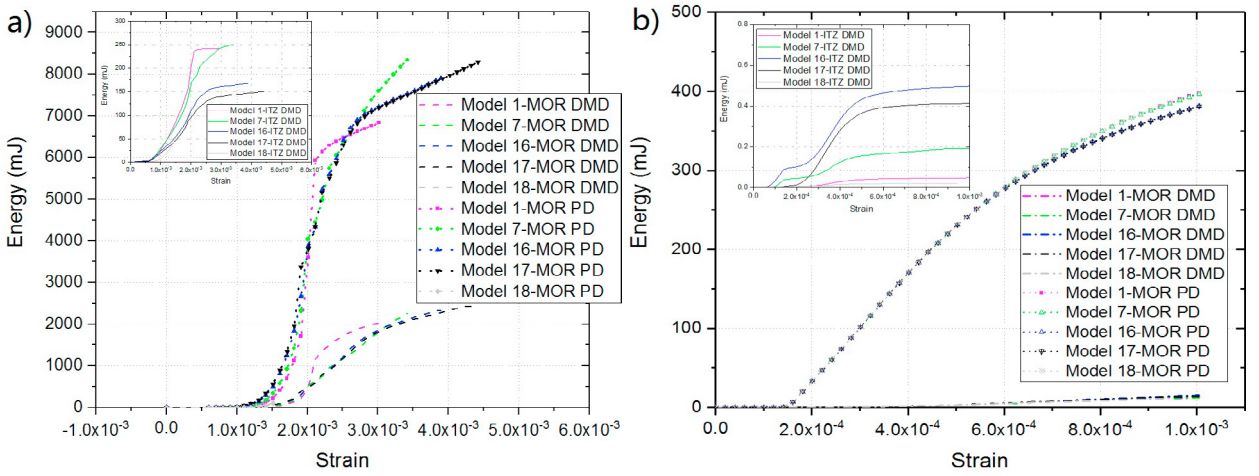

Fig. 2. Dissipated energy with variable ITZ cohesive strength under compression (a) and tension (b), where inserts show damage by ITZ

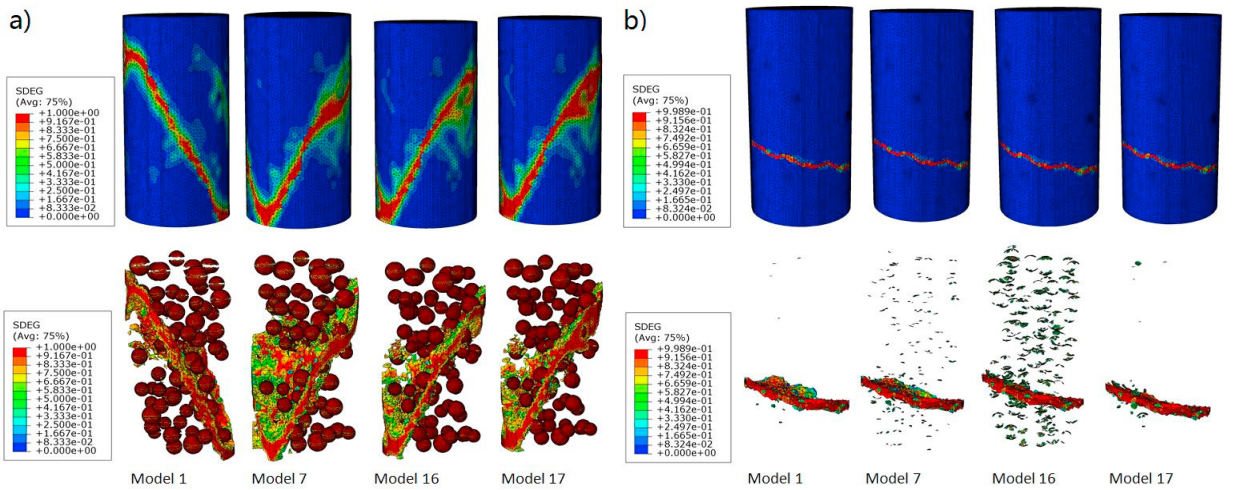

Fig. 3. Crack patterns of critical stress effect under compression (a) and tension (b) for whole model and damaged elements

complete failure. It can be seen that in compression (Fig. 1a), both normal and shear cohesive strengths have a significant effect on the predicted concrete strength. As the normal ITZ strength increases, see Models 16, 7 and 1, the concrete strength grows by 11% from 32 to 36 MPa. Comparison with experimental data suggests that the normal ITZ strength is close to the mortar tensile strength of 3.7 MPa, as presented by Model 1. As the shear cohesive strength increases, see Models 17, 1 and 18, the concrete strength grows by 18% from 31 to 38 MPa. This is in agreement with the work by [7], who compared shear strengths between one and six times the normal strength of 2.7 MPa and found increasing compressive strength. The results presented here, suggest that a shear strength three times of the normal strength (Model 1) is a good approximation. Further, Model 1 experiences more rapid softening than Models 7 and 16, i.e. the larger the normal cohesive strength for the same cohesive energy, the faster the softening. This can be linked to the energy dissipation and failure patterns: the plastic and damage dissipations are faster in Model 1 (Fig. 2a), leading to the rapid softening (Fig. 1a) and the most localised crack pattern (Fig. 3a). This crack pattern is closest to the experiment. Noted that the failure patterns of Models 18 are the same as Model 17 in compression and tension.

According to the results in tension, the normal cohesive strength does not affect the stress-strain curve (Fig. 1b), and crack patterns (Fig. 3b), which contradicts previous studies of tensile failure by [3–6]. However, in all these studies the continuum elements covering mortar and aggregate phases were assumed to have elastic behaviour, while energy

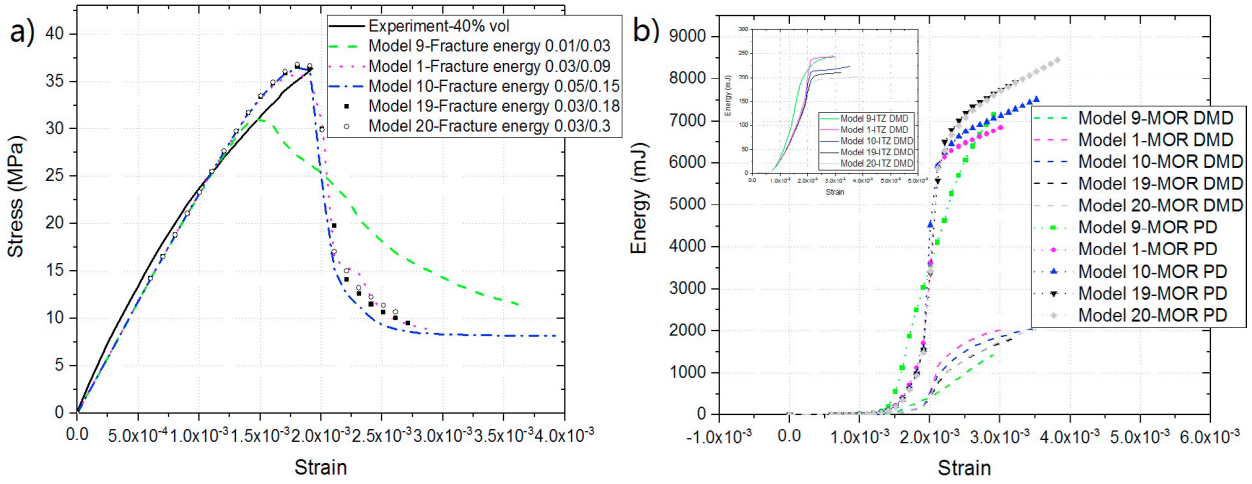

Fig. 4. Stress-strain curve (a) and dissipated energy (b) with variable ITZ fracture energy under compression, where inserts show damage by ITZ

was dissipated only by damage of cohesive elements, either along ITZ and between mortar elements [3, 6], or along ITZ and between mortar and aggregate elements [4, 5]. The introduction of damage-plasticity behaviour of mortar in the present work, which is critical for capturing the compressive behaviour with the same material parameters, changes the tensile behaviour. Firstly, a crack pattern with one dominant crack is observed (Fig. 3b), unlike the previous studies, where more than one cracks could be predicted to develop. This is in qualitative agreement with our tensile experiments. The energy dissipation is dominated by mortar plasticity (Fig. 2b) and as the ITZ normal cohesive strength increases, ITZ elements are less damaged seen by comparing Models 16, 7 and 1 in Fig. 2b and 3b. The presented results suggest that the mortar damage-plasticity plays a role in localising the damage into a dominant crack faster with increasing ITZ cohesive strength. A rough estimate of the concrete fracture energy predicted by the present model can be made by using the total work up to specimen failure and the specimen cross-section, giving 203 N/mm. This is in very good agreement with experimentally determined fracture energy for the same type of concrete [11], which provides a strong support to the proposed modelling.

Results obtained by compression with variable ITZ normal and shear fracture energy are shown in Fig. 4 and 5. It can be seen that the use of very low ITZ fracture energy (Model 9) does not provide good agreement with the experimental data (Fig. 4a). The effect of ITZ normal fracture energy is deduced by comparing the results of Models 9, 1 and 10 in Fig. 4b. The significant reduction of the concrete compressive strength for small normal fracture energy, Model 9, is due to earlier development of damage in ITZ and mortar and plastic dissipation in mortar. However, the energy dissipation rates are lower than in Model 1, resulting in an unrealistic crack pattern, as mortar plasticity and damage are not able to localise the evolution (Fig. 5a). For large normal fracture energies, Models 10, 19 and 20, the onsets of energy dissipation are similar to Model 1, resulting in similar pre-peak behaviour, but the damage dissipation is smaller, resulting again in unrealistic localisation of cracks (Fig. 5a). By comparing results with different ITZ shear fracture energy, Models 1, 19 and 20, it is shown that large mode II to mode I ratios, such as 6 or 10, lead to increased plastic dissipation in mortar, but reduced damage in ITZ and mortar (Fig. 4a). As for large normal energies, this leads to unrealistic localisation of cracks (Fig. 4b). ITZ's normal and shear fracture energy have negligible effect on the concrete tension behaviour, i.e. stress-strain curve, crack pattern and energy release.

4. Conclusions

Meso-structural models of concrete are constructed using experimentally measured mortar behaviour. Calibration of ITZ cohesive behaviour is carried out by parametric study of the effects of the normal and shear cohesive strengths and fracture energies on the concrete tensile and compressive behaviour. The main findings are as follows. Mortar plasticity and damage dominate the energy dissipation in both tension and compression. In tension, this dominance is translated into independence of stress-strain behaviour from ITZ cohesive parameters, and fast localisation of damage

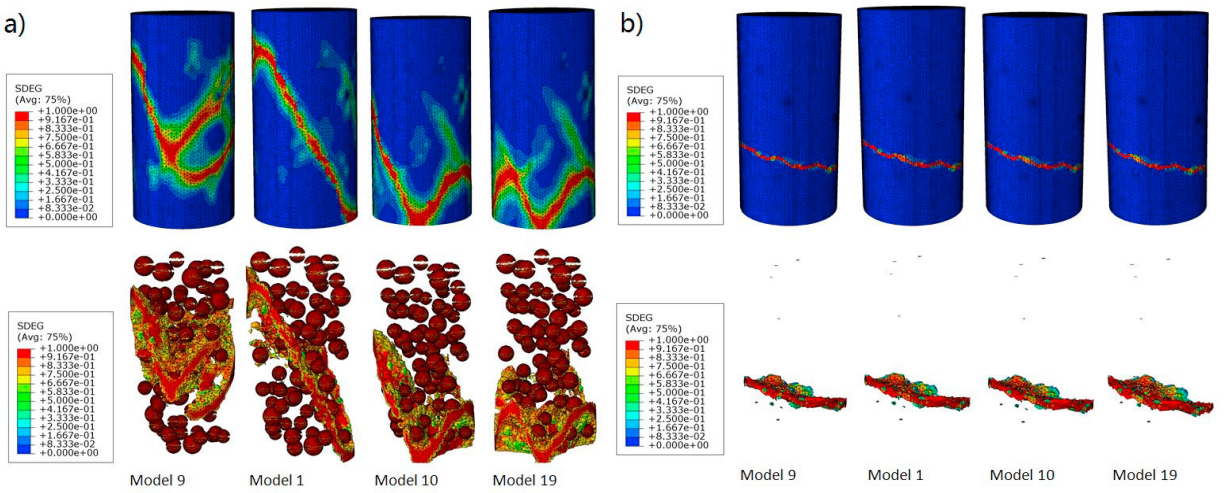

Fig. 5. Crack patterns of fracture-energy effect under compression (a) and tension (b) for whole model and damaged elements

into a dominant crack. The localisation is governed by mortar damage. In compression, the stress-strain behaviour is affected by the ITZ cohesive parameters - increasing ITZ cohesive strength and fracture energy increases concrete strength. The results suggest: ITZ normal cohesive strength close to the mortar tensile strength and cohesive energy of 0.03 N/mm; ratio between ITZ shear and normal cohesive strengths approximately three.

Acknowledgements

Wang acknowledges the support of Manchester X-ray Imaging Facility for using Aviso and Simpleware and IT Services for using Computational Shared Facility (CSF). Jivkov acknowledges gratefully the financial support of EPSRC via grant EP/N026136/1.

References

[1] W. A. Tasong, C. J. Lynsdale, J. C. Cripps, Aggregate-cement paste interface: Part I. Influence of aggregate geochemistry, Cem. Concr. Res. 29 (1999) 1019–1025. doi:10.1016/S0008-8846(99)00086-1. arXiv:arXiv:1011.1669v3.

[2] J. Xiao, W. Li, D. J. Corr, S. P. Shah, Effects of interfacial transition zones on the stress-strain behavior of modeled recycled aggregate concrete, Cem. Concr. Res. 52 (2013) 82–99. doi:10.1016/j.cemconres.2013.05.004.

[3] C. M. López, I. Carol, A. Aguado, Meso-structural study of concrete fracture using interface elements. I: numerical model and tensile behavior, Mater. Struct. 41 (2008) 583–599. doi:10.1617/s11527-007-9314-1.

[4] W. Ren, Z. Yang, R. Sharma, C. Zhang, P. J. Withers, Two-dimensional X-ray CT image based meso-scale fracture modelling of concrete, Eng. Fract. Mech. 133 (2015) 24–39. doi:10.1016/j.engfracmech.2014.10.016.

[5] X. Wang, M. Zhang, A. P. Jivkov, 3-Computational technology for analysis of 3D meso-structure effects on damage and failure of concrete, Int. J. Solids Struct. 80 (2016) 310–333. doi:10.1016/j.ijsolstr.2015.11.018.

[6] W. Trawiński, J. Tejchman, J. Bobiński, A three-dimensional meso-scale modelling of concrete fracture, based on cohesive elements and X-ray μCT images, Eng. Fract. Mech. 189 (2018) 27–50. doi:10.1016/j.engfracmech.2017.10.003.

[7] R. Zhou, Y. Lu, A mesoscale interface approach to modelling fractures in concrete for material investigation, Constr. Build. Mater. 165 (2018) 608–620. doi:10.1016/j.conbuildmat.2018.01.040.

[8] J. Wang, A. P. Jivkov, D. L. Engelberg, Q. Li, Meso-scale modelling of mechanical behaviour and damage evolution in normal strength concrete, Procedia Struct. Integr. 13 (2018) 560–565. doi:10.1016/j.prostr.2018.12.092.

[9] GB50010, Chinese code for the design of reinforced concrete structures, 2010.

[10] W. Trawiński, J. Bobiński, J. Tejchman, Two-dimensional simulations of concrete fracture at aggregate level with cohesive elements based on X-ray μCT images, Eng. Fract. Mech. 168 (2016) 204–226. doi:10.1016/j.engfracmech.2016.09.012.

[11] J. Lee, M. M. Lopez, An Experimental Study on Fracture Energy of Plain Concrete, Int. J. Concr. Struct. Mater. 8 (2014) 129–139. doi:10.1007/s40069-014-0068-1.